Tests and finite element analysis on the local buckling of 420 MPa steel equal angle columns under axial compression

G. Shi*[1], Z. Liu[2], H.Y. Ban[1], Y. Zhang[2], Y.J. Shi[1], and Y.Q. Wang[1]

[1]*Key Laboratory of Civil Engineering Safety and Durability of China Education Ministry, Department of Civil Engineering, Tsinghua University, Beijing 100084, P.R. China*
[2]*School of Civil Engineering, Beijing Jiaotong University, Beijing 100044, P.R. China*

(Received September 09, 2010, Revised July 23, 2011, Accepted October 14, 2011)

Abstract. Local buckling can be ignored for hot-rolled ordinary strength steel equal angle compression members, because the width-to-thickness ratios of the leg don't exceed the limit value. With the development of steel structures, Q420 high strength steel angles with the nominal yield strength of 420 MPa have begun to be widely used in China. Because of the high strength, the limit value of the width-to-thickness ratio becomes smaller than that of ordinary steel strength, which causes that the width-to-thickness ratios of some hot-rolled steel angle sections exceed the limit value. Consequently, local buckling must be considered for 420 MPa steel equal angles under axial compression. The existing research on the local buckling of high strength steel members under axial compression is briefly summarized, and it shows that there is lack of study on the local buckling of high strength steel equal angles under axial compression. Aiming at the local buckling of high strength steel angles, this paper conducts an axial compression experiment of 420MPa high strength steel equal angles, including 15 stub columns. The test results are compared with the corresponding design methods in ANSI/AISC 360-05 and Eurocode 3. Then a finite element model is developed to analyze the local buckling behavior of high strength steel equal angles under axial compression, and validated by the test results. Following the validation, a finite element parametric study is conducted to study the influences of a range of parameters, and the analysis results are compared with the design strengths by ANSI/AISC 360-05 and Eurocode 3.

Keywords: local buckling; high strength; steel equal angle; axial compression; Q420; finite element analysis.

1. Introduction

The development of steel construction is always closely linked to advancement in steel materials and their production methods. Only in the recent years, a new kind of steel with high yield strength as well as good fabrication properties such as weldability has been introduced into the construction market (IABSE 2005). Currently with the development of steel structures, the use of high strength steel in building and bridge constructions has increased very rapidly in the world, such as Japan, Europe, the USA, Australia and China, because of the considerable gains in many aspects (Pocock 2006, Shi and Bijlaard 2007), and Q420 steel angle members with the nominal yield strength of 420 MPa have also been used in many steel structures in China, especially in transmission towers and long span trusses. Compared with ordinary strength steel, high strength steel has many advantages especially when applied

* Corresponding author, Ph, D., E-mail: shigang@tsinghua.edu.cn

in compression members, such as increased load-carrying capacity at reduced cost. So it is believed that high strength steel will be used more frequently in longer bridge spans, taller buildings and larger offshore platforms in the future.

Based on the corresponding regulations in the steel structures design codes of many countries, local buckling behavior can be ignored for steel equal angle columns of normal strength with typical cross-sectional dimensions, because the width-to-thickness ratio of the leg doesn't exceed the limit value of the ratio, which is related to the steel strength. But with the increase of the steel strength, the limit value of the width-to-thickness ratio against local buckling decreases. Consequently, the width-to-thickness ratios of the legs for high strength steel equal angles often exceed the limit value, which does not satisfy the requirement of against local buckling. Hence local buckling is more critical for high strength steel equal angle members under axial compression, especially for those with small slenderness.

Some tests and finite element analysis on the local buckling behavior of high strength steel members under axial compression have been conducted. Nishino *et al.* (1967) presented an experimental study of the effect of residual stress on the local buckling strength of component plates of welded built-up box columns. The test consisted of four sets of short columns, of which two were made from ASTM A7 steel (f_y = 235 MPa) and the other two were made from ASTM A514 steel (f_y = 690 MPa). The test results show that the most important factor in the analysis of the effect of residual stress on the local buckling strength is the ratio of the compressive residual stress to the steel yield stress, rather than the magnitude of the compressive residual stress. So the effect of residual stress on the local buckling strength is less pronounced for high strength steel than it is for ordinary strength steel.

Rasmussen and Hancock (1992) reported an experimental program on stub columns fabricated from BISALLOY 80 steel plates (equivalent to ASTM A514 steel, f_y = 690 MPa), including three types of cross section: square box section, cruciform section and I-section. The test results confirm the conclusion previously drawn for ordinary strength steel (Dwight and Moxham 1969) that the interaction between component plates is insignificant at the ultimate load so that the compressive strength of a cross section can be determined by considering the plates individually. Another conclusion is that the yield slenderness limit in AS 4100 (1998), which demarcates slender and non-compact flanges of compressed cross sections, is the same for ordinary and high strength steel.

Tang and Mahendran (2004) conducted a numerical investigation into the interactive effect of local buckling on I-section columns fabricated from BISALLOY 80 steel plates. The finite element model was validated by the tests conducted by Rasmussen and Hancock (1992). The parametric study results indicate that the interactive effect of local buckling between the component plate elements within the cross section exists, and influence the load-carrying capacity of the section. Furthermore, the slenderness limit recommended in AS 4100 (1998) is not appropriate for welded structural sections made of high strength steel. The two conclusions are both contradictory to that drawn by Rasmussen and Hancock (1992).

Clarin and Lagerqvist (2005) presented a test program on the local buckling of box section stub columns, which were fabricated from steel with the nominal yield stress of 420, 700 and 1,100 MPa, to verify whether the Winter function in Eurocode 3 (EN 1993-1-5 2006) is applicable to high strength steel. The test results suggest that simply supported plates made of high strength steel have no different behavior regarding the buckling resistance than ordinary strength steel. The behavior of high strength steel may even coincide better with the Winter function than that of ordinary strength steel. This implies that the residual stress magnitudes in welded plates of high strength steel may not be that different than in plates made of ordinary strength steel.

Usami and Fukumoto (1982) reported an experimental study on the local and overall interaction

buckling strength of welded built-up box columns fabricated from HT80 steel (equivalent to ASTM A514 steel, $f_y = 690$ MPa). Based on the test results and the AISC Q-factor method, a simple design formula is presented to predict, with good accuracy, the local and overall interaction buckling strength of both centrally and eccentrically loaded box columns. Besides, it is concluded that in high strength steel columns, an economical design is probably obtained when the cross section is proportioned in such a way that local plate buckling is permitted to occur.

In conclusion, the existing research results show that the effect of geometric imperfection and residual stress on the local buckling strength of members under axial compression is less pronounced for high strength steel than it is for ordinary strength steel. So the local buckling strength of high strength steel members under axial compression may be enhanced. Furthermore, the existing research results are all based on welded box, cruciform or I-section, excluding the steel equal angle. That is to say, there is a lack of study on the local buckling behavior of high strength steel equal angle members under axial compression, which makes it necessary to perform a systematic study with both experimental and numerical investigations.

Aiming at the local buckling behavior of high strength steel equal angles, this paper introduces an axial compression experiment of 420 MPa high strength steel equal angle columns, with the total number of 15 specimens, including 5 different sections, with small slenderness, whose width-to-thickness ratios of the leg all exceed the limit values specified in many countries' steel structures design codes. The test results are compared with the corresponding design strengths in the American code ANSI/AISC 360-05 (2005) and Eurocode 3 (EN 1993-1-5 2006, EN 1993-1-1 2005). Then a finite element model is developed in this paper with the general-purpose finite element software ANSYS with incorporation of the residual stresses and the initial geometric imperfections of the specimens, to analyze the local buckling behavior of high strength steel equal angle columns under axial compression. This paper presents the key details of the finite element modeling. Then the finite element model is validated by the test results. Following the validation, a range of influential parameters are investigated to study their effects on the local buckling behavior of high strength steel equal angle columns under axial compression, and the results are compared with the design strengths by ANSI/AISC 360-05 and Eurocode 3, which provides a reference for the related design.

2. Test program

2.1. Test specimens

The test was performed on 420MPa steel equal angle stub columns of 5 different section sizes, i.e., L125 × 8, L140 × 10, L160 × 10, L180 × 12 and L200 × 14. For each section size, 3 specimens were tested, so that the test program comprised a total of 15 stub column specimens. The slenderness of all the specimens, about the weak axis x, as shown in Fig. 1, was equal to 10, to ensure that the overall buckling behavior was excluded.

The test specimens have been labeled so that the section size and the specimen can be identified from the label. The first letter of the label 'L' represents the steel equal angle. The next two numbers following the first letter signify the width of the section and the thickness of the leg respectively. The last character of the label identifies the serial number of specimens with the same section size, and is '1', '2' or '3', since 3 specimens were tested for each section size.

The nominal and measured dimensions of each stub column specimen are shown in Table 1, where

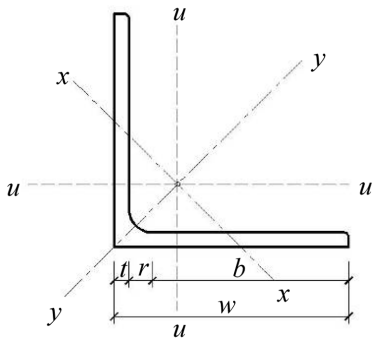

Fig. 1 Definition of symbols

Table 1 Nominal and measured dimensions of test specimens

Specimen	l (mm)				w (mm)			t (mm)		
	nominal	$x=1$	$x=2$	$x=3$	$x=1$	$x=2$	$x=3$	$x=1$	$x=2$	$x=3$
L125×8-x	250	249.8	250.3	250.3	125.0	125.1	124.9	7.965	7.880	7.930
L140×10-x	278	277.5	278.2	277.9	139.9	140.0	140.1	10.010	9.990	10.005
L160×10-x	320	319.5	319.5	320.0	160.3	159.8	160.2	9.915	9.910	9.905
L180×12-x	358	355.9	359.3	358.2	179.6	179.6	179.7	11.880	11.880	11.885
L200×14-x	398	398.2	399.2	398.9	201.1	200.6	200.8	13.530	13.785	13.540

the symbols used are defined in Fig. 1. The symbols 'l', 'w' and 't', whose measurements are based on the average values, signify the length of the column, the width of the section and the thickness of the leg respectively.

2.2. Test configurations

The stub columns were tested between pinned end bearings in a servo-controlled test rig. The instrumentation of the pin-ended stub columns consisted of a load cell measuring the axial force, displacement transducers and strain gauges. The test configuration is shown in Fig. 2. The ends of the test specimens were milled flat before testing to allow proper seating on the end plates with the dimensions of 350 mm × 200 mm × 40 mm, as shown in Fig. 3, and then on the rigid end platens of the testing rig. The ear plate in Fig. 3 is just used to restrain the horizontal displacement of the stub column, and the plate of specimens can be freely deformed.

For each specimen, 6 strain gauges were attached at the mid-length to measure the longitudinal strains, and their positions in the section are shown in Fig. 4, labeled from '2-1' to '2-6'. Two displacement transducers attached to the top end plate, labeled '1-1' and '1-2', were to measure the longitudinal displacement, and another two displacement transducers attached at the mid-length, labeled '1-3' and '1-4', were to measure the transversal displacement. Their positions are also shown in Fig. 4.

Overall geometric imperfections in this paper are defined as the deviation of three edge lines of the angle column at the mid-length from a relevant straight line connecting the ends, and are denoted by v_{01}, v_{02}, v_{03} and v_{04}, as shown in Fig. 5. The measured geometric imperfection values of each stub column specimen are shown in Table 2, where the last column v is the torsional geometric imperfection

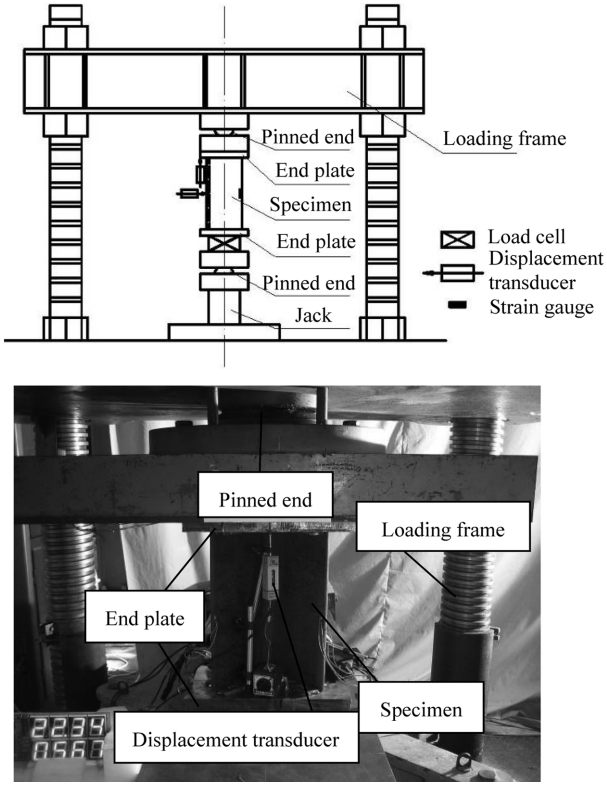

Fig. 2 Test configuration

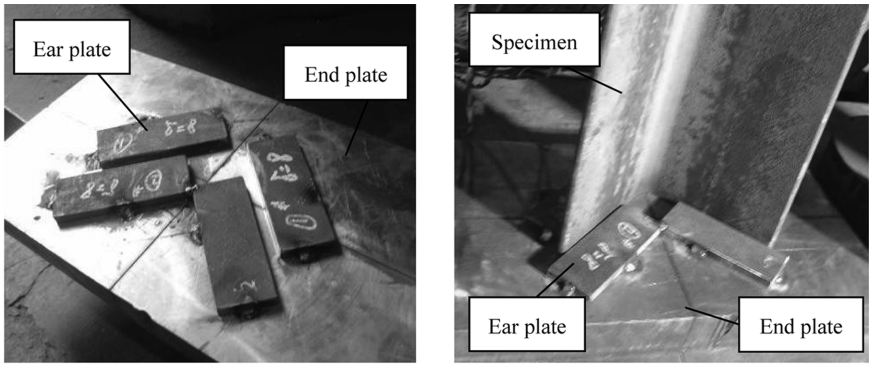

Fig. 3 Photographs of the end plate

as the local buckling occurs. Since the cross section at the mid-length will rotate about its shear center when the local buckling deformation of the specimen occurs, the geometric imperfection value v is defined as Eq. (1)

$$v = \max[\mathrm{abs}(v_{01} - v_{02}), \mathrm{abs}(v_{03} - v_{04})] \tag{1}$$

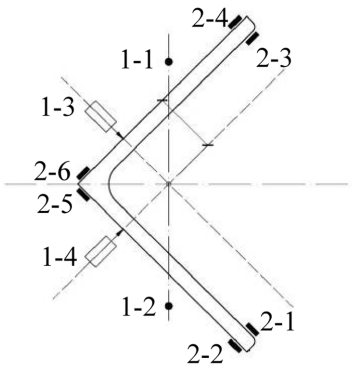

Fig. 4 Layout of measuring points

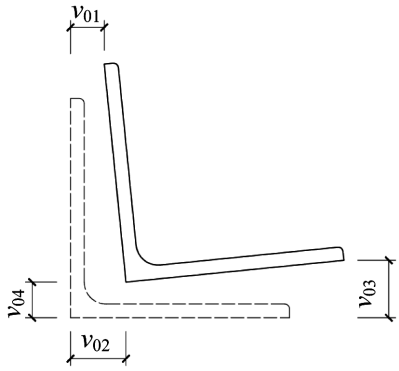

Fig. 5 Geometric imperfections

Table 2 Measured geometric imperfection values of test specimens (mm)

Specimen	v_{01}	v_{02}	v_{03}	v_{04}	v
L125×8-1	1.020	1.040	1.900	0.840	1.060
L125×8-2	1.180	0.880	1.480	0.900	0.580
L125×8-3	1.380	1.020	0.860	0.700	0.360
L140×10-1	0.800	1.280	0.820	0.920	0.480
L140×10-2	1.180	0.680	0.720	1.020	0.500
L140×10-3	1.320	1.220	1.480	0.960	0.520
L160×10-1	1.000	0.840	0.830	0.980	0.160
L160×10-2	1.040	1.000	1.940	1.120	0.820
L160×10-3	0.720	0.820	1.000	0.580	0.420
L180×12-1	0.460	0.800	1.420	0.280	1.140
L180×12-2	0.280	0.660	1.040	0.520	0.520
L180×12-3	0.480	1.700	1.460	0.560	1.220
L200×14-1	1.060	0.400	0.700	0.200	0.660
L200×14-2	0.840	0.780	1.300	0.860	0.440
L200×14-3	0.900	0.920	0.840	0.820	0.020

2.3. Tension coupon tests

For each angle section, 3 tension coupons were prepared for the tension tests, to obtain the mechanical properties of the steel angles. The labels for the coupons signify the section size of angles where they were cut from. The first two letters of the label 'TL' mean the tension coupon of the angle. The following number represents the section size, and the last character of the label identifies the serial number of tension coupons with the same section size. The dimensions of tension coupons and their cutting locations in the angle legs are all based on the Chinese mechanical testing codes (GB/T 228-2002 2002, GB/T 2975-1998 1998).

The tension coupons were cut parallel to the rolling direction and equipped with two strain gauges on opposite sides at the mid-length to measure the longitudinal strains. An extensometer was also attached on each coupon at the middle part to measure the longitudinal deformation, which can be used to

measure accurate strains after strain gauges fail due to the excessive deformation.

The stress-strain curves obtained from tension coupon tests are shown in Fig. 6~Fig. 10 for L125 × 8,

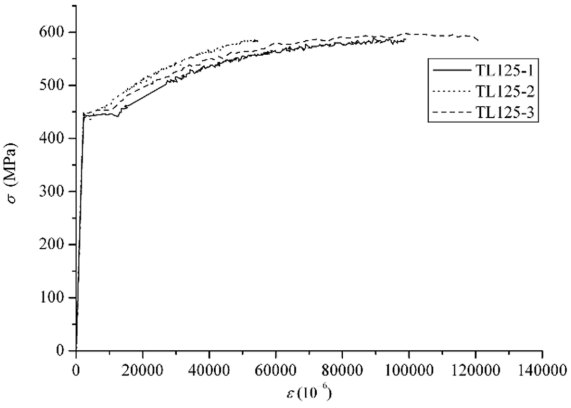

Fig. 6 Stress-strain curves for L125 × 8 section

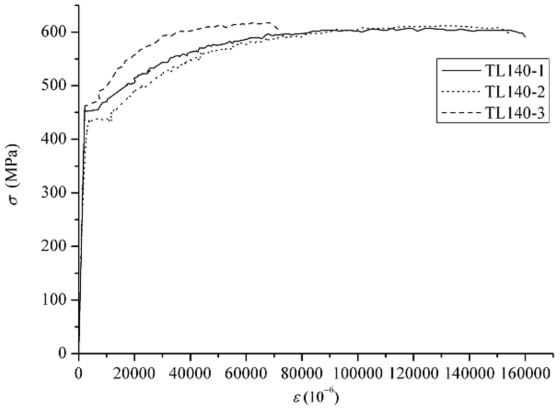

Fig. 7 Stress-strain curves for L140 × 10 section

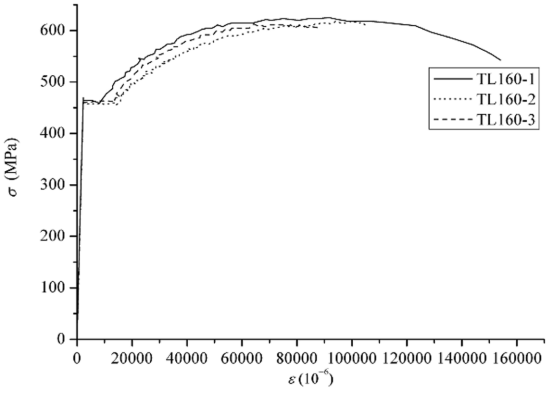

Fig. 8 Stress-strain curves for L160 × 10 section

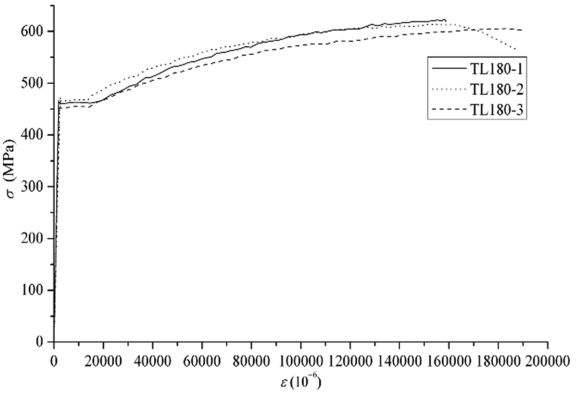

Fig. 9 Stress-strain curves for L180 × 12 section

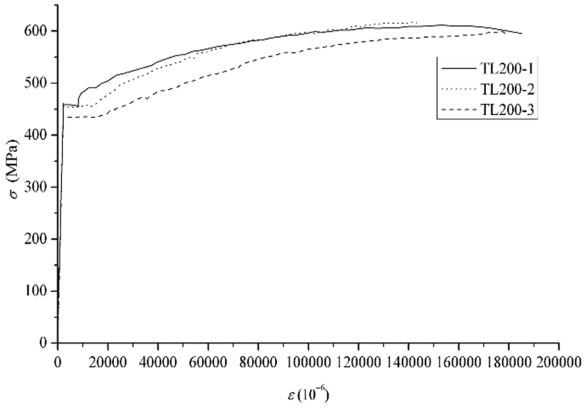

Fig. 10 Stress-strain curves for L200 × 14 section

Table 3 Mechanical properties of steel angles

Section	f_y (MPa)	f_u (MPa)	ε_1	ε_2	ε_3
L125×8	442.1	595.0	0.002143	0.009940	0.080241
L140×10	449.1	612.0	0.002180	0.007221	0.101628
L160×10	460.7	618.6	0.002236	0.012089	0.084875
L180×12	459.4	614.4	0.002234	0.014297	0.164464
L200×14	448.8	609.0	0.002179	0.012218	0.157580

L140 × 10, L160 × 10, L180 × 12 and L200 × 14 sections, respectively. In these figures, the strain ε is the average of the two strain gauge readings and the stress σ is the measured load divided by the initial area, which was calculated from the tension coupon's dimensions measured before testing. The strains greater than 20,000 $\mu\varepsilon$ were obtained from the longitudinal deformation, which was calculated from the extensometer readings divided by the standard distance 50 mm of the extensometer.

The mechanical properties obtained from the tension coupon tests are shown in Table 3, where f_y is the yield strength and f_u is the ultimate strength. It can be seen from the table that for all the steel angles, the measured values of the yield strength exceed the nominal value 420 MPa.

3. Test results

The measured ultimate loads P_u of all the specimens are shown in Table 4, and the representative stub column failure mode after testing is shown in Fig. 11. All the specimens have the local buckling deformation.

The representative load-transverse displacement curves of the specimens are shown in Fig. 12, where "1-3" and "1-4" stand for the transverse displacements measured by the two displacement transducers attached at the mid-length, as defined in Fig. 4. From Fig. 12 it can be seen that at the beginning of the loading, the two displacements which increase together are almost equal, and the two curves almost coincide. When the load reaches point A in the figure, one of the displacements keeps increasing while the other begins to decrease, and the two curves separate, which indicates the occurrence of the local buckling in the specimen. Then the local buckling develops with the loading until the ultimate load, i.e., point B in the figure, where the specimen reaches the ultimate state. After that, the load begins to decrease, which shows that the specimen loses the load-carrying capacity.

According to the Chinese steel structures design code GB 50017-2003 (2006), the limit value of the

Table 4 Measured ultimate loads

Specimen	Measured ultimate loads P_u (kN)			
	$x = 1$	$x = 2$	$x = 3$	Average
L125×8-x	854.9	817.1	851.5	841.2
L140×10-x	1181.3	1232.1	1224.1	1212.5
L160×10-x	1361.2	1415.3	1378.1	1384.9
L180×12-x	1904.4	1880.6	1829.4	1871.4
L200×14-x	2362.2	2348.8	2417.0	2376.0

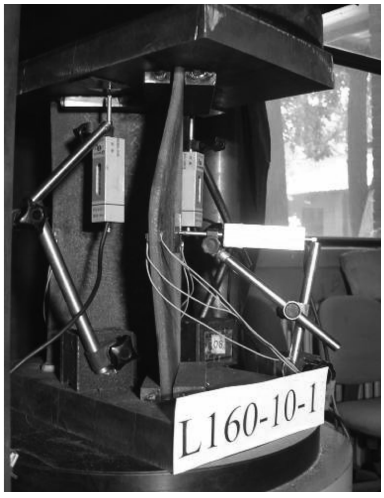

Fig. 11 Representative columns after testing (Specimen L160 × 10-1)

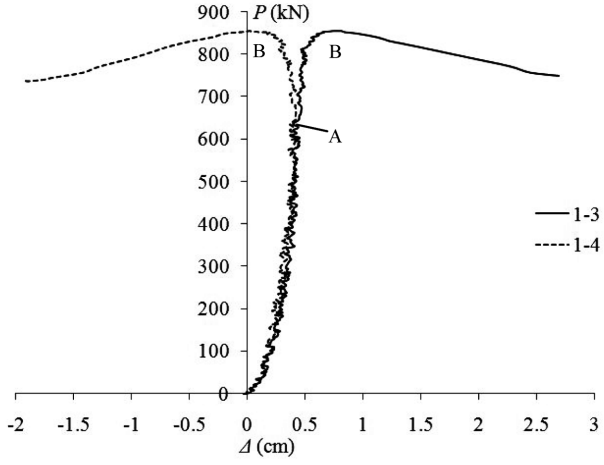

Fig. 12 Load-transverse displacement curves

width-to-thickness ratio $(b/t)_{\lim}$ for hot-rolled steel equal angle compression members is determined as Eq. (2)

$$(b/t)_{\lim} = (10 + 0.1\lambda)\sqrt{235/f_y} \tag{2}$$

Where $30 \le \lambda \le 100$ denotes the slenderness of the member and f_y denotes the steel yield strength.

The width-to-thickness ratio b/t (defined in Fig. 1) of all the sections and its limit value calculated by Eq. (2) ($\lambda = 30$) are shown in Table 5, from which it can be seen that the width-to-thickness ratio values all exceed the limit value, so that the local buckling behavior must be considered.

The ultimate stress σ of all the specimens, which is obtained by dividing the ultimate load P_u by the section area A, and the comparison with the measured yield strength f_y (seen in Table 3) are shown in Table 6.

From Table 6 it can be seen that the ultimate stresses of all the specimens, except for L140 × 10-2, are

Table 5 Width-to-thickness ratio values and the limit value

Section	w (mm)	b (mm)	t (mm)	w/t	b/t	$(b/t)_{\lim}$	$(b/t)/(b/t)_{\lim}$
L125×8	125	103	8	15.62	12.88	9.72	1.32
L140×10	140	116	10	14.00	11.60	9.72	1.19
L160×10	160	134	10	16.00	13.40	9.72	1.38
L180×12	180	152	12	15.00	12.67	9.72	1.30
L200×14	200	168	14	14.28	12.00	9.72	1.23

Table 6 Ultimate stresses

Specimen	Ultimate stresses σ (MPa)				σ/f_y			
	$x=1$	$x=2$	$x=3$	Average	$x=1$	$x=2$	$x=3$	Average
L125×8-x	432.9	413.7	431.1	425.9	0.979	0.936	0.975	0.963
L140×10-x	431.6	450.1	447.2	443.0	0.961	1.002	0.996	0.986
L160×10-x	432.1	449.3	437.5	439.6	0.938	0.975	0.950	0.954
L180×12-x	450.8	445.2	433.1	443.0	0.981	0.969	0.943	0.964
L200×14-x	432.3	429.9	442.3	434.8	0.963	0.958	0.986	0.969

lower than the corresponding steel yield strength, which indicates that the local buckling appears before the steel yielding. Therefore, the local buckling is significant for the 420 MPa high strength steel equal angle members under axial compression with small slenderness, whose width-to-thickness ratio values exceed the limit value, and it is the local buckling strength that determines their ultimate strength. Besides, the ratio values σ/f_y differ more or less with different width-to-thickness ratios. The specimens of section L160 × 10 have the largest width-to-thickness ratio value, and their ratio values σ/f_y are the smallest on average. While the specimens of section L140 × 10 have the smallest width-to-thickness ratio value, and their ratio values σ/f_y are the largest on average. It shows that with the decrease of the width-to-thickness ratio the local buckling strength increases.

4. Design methods of current codes

The test results are compared with the corresponding design strengths by ANSI/AISC 360-05 (2005) and Eurocode 3 (EN 1993-1-5 2006, EN 1993-1-1 2005), which are introduced firstly.

Sections are classified as compact, noncompact and slender-element sections in ANSI/AISC 360-05 (2005). Compact sections are capable of developing a fully plastic stress distribution. Noncompact sections can develop partial yielding in compression elements before local buckling occurs, but will not resist inelastic local buckling at the strain levels required for a fully plastic stress distribution. Slender-element sections have one or more compression elements that will buckle elastically before the yield stress is achieved.

For single angle compression members, the limit value of the width-to-thickness ratio is determined as Eq. (3)

$$\lambda_r = 0.45\sqrt{E/F_y} \tag{3}$$

where F_y denotes the steel yield strength. If the width-to-thickness ratio w/t (defined in Fig. 1) of the

angle leg does not exceed λ_r, the section is noncompact. Otherwise the section is referred to as a slender-element section.

For 420 MPa high strength steel angles, the limit value of the width-to-thickness ratio is 9.97 according to Eq. (3) (F_y = 420 MPa). From Table 5 it can be seen that the width-to-thickness ratio values of the five sections all exceed the limit value 9.97. Based on ANSI/AISC 360-05, the five sections all belong to the slender-element section. That is to say, the local buckling will occur before the steel yielding, which is consistent with the test results.

The plate strength is obtained as the reduction factor Q_s for single angle compression members with slender sections

$$\text{When } w/t \le 0.45\sqrt{E/F_y}, Q_s = 1.0 \tag{4}$$

$$\text{When } 0.45\sqrt{E/F_y} < w/t \le 0.91\sqrt{E/F_y}, Q_s = 1.34 - 0.76\left(\frac{w}{t}\right)\sqrt{\frac{F_y}{E}} \tag{5}$$

$$\text{When } w/t > 0.91\sqrt{E/F_y}, Q_s = \frac{0.53E}{F_y(b/t)^2} \tag{6}$$

Four classes of cross sections are defined in Eurocode 3 (EN 1993-1-1 2005), as follows: Class 1 cross sections are those which can form a plastic hinge with the rotation capacity required from plastic analysis without reduction of the resistance. Class 2 cross sections are those which can develop their plastic moment resistance, but have limited rotation capacity because of local buckling. Class 3 cross sections are those in which the stress in the extreme compression fiber of the steel member assuming an elastic distribution of stresses can reach the yield strength, but local buckling is liable to prevent development of the plastic moment resistance. Class 4 cross sections are those in which local buckling will occur before the attainment of yield stress in one or more parts of the cross section.

For single angle compression members, the limit value of the width-to-thickness ratio is determined as Eq. (7)

$$[w/t] = 15\sqrt{235/f_y} \tag{7}$$

where f_y denotes the steel yield strength. If the width-to-thickness ratio w/t (defined in Fig. 1) of the angle leg does not exceed $[w/t]$, the section is taken as Class 3 section. Otherwise the section should be treated as Class 4 section.

For 420 MPa high strength steel angles, the limit value of the width-to-thickness ratio is 11.22 according to Eq. 7 (f_y = 420 MPa), which is larger than the limit value by ANSI/AISC 360-05. From Table 5 it can be seen that the width-to-thickness ratio values of the five sections all exceed the limit value 11.22. Based on Eurocode 3, the five sections are all classified as Class 4 section. It means that the local buckling will occur before the steel yielding, which is consistent with the test results and the classification by ANSI/AISC 360-05.

The plate strength is obtained as the reduction factor ρ for Class 4 section (EN 1993-1-5 2006)

$$\text{When } \bar{\lambda}_p \le 0.748, \rho = 1.0 \tag{8}$$

$$\text{When } \bar{\lambda}_p > 0.748, \rho = \frac{\bar{\lambda}_p - 0.188}{\bar{\lambda}_p^2} \tag{9}$$

$$\text{where } \bar{\lambda}_p = \frac{w/t}{28.4\sqrt{235/f_y}\sqrt{k_\sigma}} \tag{10}$$

k_σ is the bucking factor, and $k_\sigma = 0.43$ for angle compression members. Eq. (9) is the Winter function.

The comparison between the nondimensional test strengths σ / f_y and the nondimensional design strengths by ANSI/AISC 360-05 (2005) and Eurocode 3 (EN 1993-1-5 2006, EN 1993-1-1 2005) is shown in Fig. 13, from which it can be seen that the test strengths are all higher than the corresponding design strengths, with an average excess of 18.09% and 27.22% respectively, and with the increase of the width-to-thickness ratio, the excess range becomes higher. The most important reason is that the effects of imperfections such as initial crookedness and residual stresses are less severe for high strength steel members, which is consistent with the existing research results. Thus, the design methods of ANSI/AISC 360-05 and Eurocode 3 can predict sufficiently safe results for the local buckling of 420 MPa high strength steel equal angle columns under axial compression, whose width-to-thickness ratio values exceed the limit value.

5. Finite element analysis

5.1. Finite element model

ANSYS (ANSYS Multiphysics 10.0 2003) has been widely used across many disciplines with well-documented success in modeling of high nonlinear phenomena, and it has been adopted to carry out the numerical investigation because of its robustness in nonlinear analysis. Element SHELL 181, which supports nonlinear buckling analysis and allows the incorporation of initial stresses, is used to develop the proposed finite element model. It is a 4-node element with 6 degrees of freedom at each node:

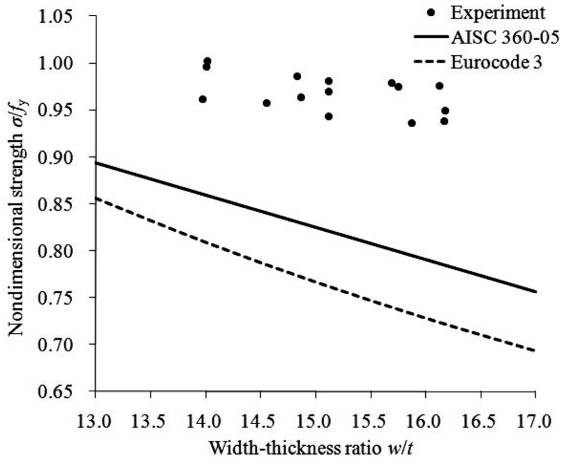

Fig. 13 Comparison between nondimensional test and design strengths

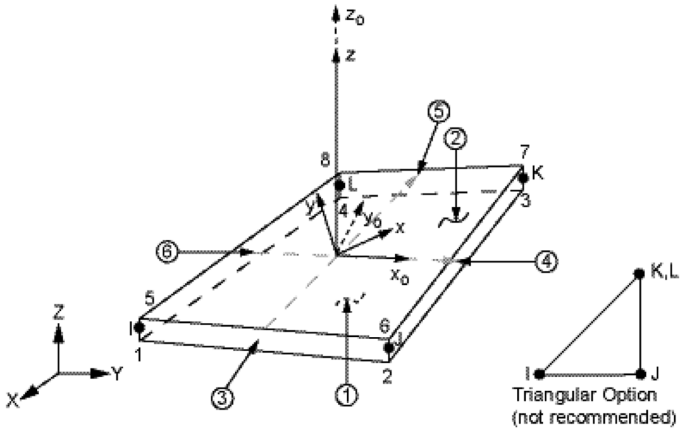

Fig. 14 Element SHELL 181

translations in the *x*, *y*, and *z* directions, and rotations about the *x*, *y*, and *z*-axes, as shown in Fig. 14. In general it is highly appropriate in linear, large rotation and large strain nonlinear analysis.

In the proposed model, an axial concentric compressive force is applied at the centroid of one end of the model. This load application will cause an artificial premature failure due to significant stress concentration in the vicinity of the load application, which is clearly a numerical problem and needs to be rectified. The method to solve this problem is to provide an end plate, with the thickness of 100 mm and linear elastic property, at both ends of the model, so that the applied load will be distributed uniformly over the cross section of the angle columns. The effect of the end plate is the same as the multiple point constraint (MPC) in ABAQUS (ABAQUS Theory Manual 2003) and the elastic strip used by Tang and Hermann (Tang and Hermann 2004, 2002). The finite element model with the end plates is shown in Fig. 15.

A mesh convergence study was carried out and two finite element meshes with 8 and 16 elements along the transverse direction of the angle section had been established to compare the accuracy of the numerical models; the finite element mesh is divided into 16 elements along the longitudinal direction.

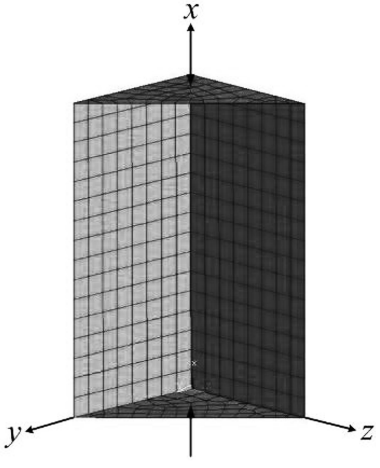

Fig. 15 Finite element model

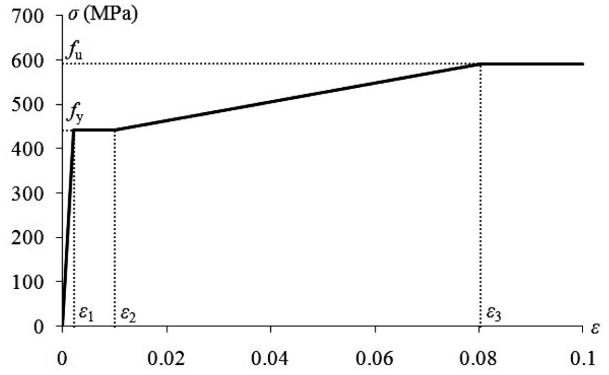

Fig. 16 Multi-linear material model

It is found that the difference between these two meshes is fairly small, and so the finite element model with 8 and 16 elements along the transverse and the longitudinal directions is adopted for all subsequent analyses.

The boundary condition for both ends of the model is assigned to be an ideal pin end. At the unloaded end, three translational degrees of freedom are restrained as well as the rotation about the longitudinal axis. The loaded end is restrained as the same as that of the unloaded end except for the translation in the longitudinal direction. All the restraints are applied to the centroid nodes in the end plates.

The von Mises failure criteria and a multi-linear material model, which is shown in Fig. 16, are adopted for all the specimens. All the values of the material parameters are derived from the tension coupon tests and they are presented in Table 3. The values of 2.06×10^5 MPa and 0.3 for the Young's modulus, E, and the Poisson ratio, v, are adopted respectively.

5.2. Initial imperfections

The finite element analysis (FEA) conducted in this paper considers the measured initial imperfections of the specimens, including the geometric imperfections and the residual stresses.

The initial geometric imperfection values v adopted in the FEA are shown in the last column of Table 2, and they are obtained by Eq. (1), as mentioned above. The shape of the geometric imperfections is set to match the preferred failure shape given by the critical buckling mode, which is also the first eigenvalue buckling mode of the angles as shown in Fig. 17.

Based on the results of the eigenvalue buckling analysis, the displacement of the cross section in the mid-length of the specimen is extracted, and the ratio of v to this displacement is input. Then the input of the geometric imperfection in the FEA is done.

For each angle section, 3 specimens were prepared for the residual stress tests, to obtain the longitudinal residual stress of the steel angles (Ban *et al.* 2009). The residual stress distributions obtained from the residual stress tests are shown in Fig. 18, where "–" denotes the compressive stress and "+" denotes the tensile stress. β is the peak value coefficient of the residual stresses and is shown in Table 7. The distribution of the measured residual stresses is consistent with that used in GB 50017-2003 (Code for design of steel structures committee 2003), but the magnitude of the measured residual stresses is obviously smaller, as shown in Table 7. From Table 7 it is shown that the magnitude of the measured residual stresses decreases with the increase of the width-to-thickness ratios of the sections,

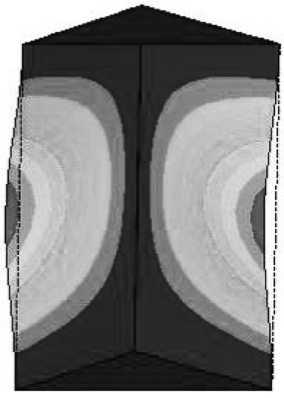

Fig. 17 Critical buckling mode

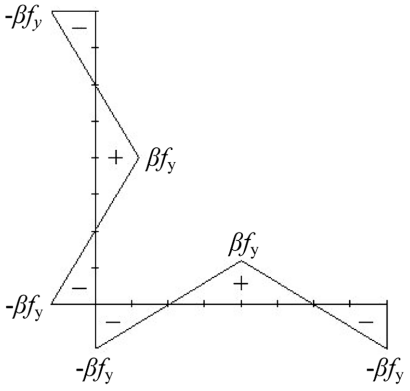

Fig. 18 Measured residual stress distribution

Table 7 Residual stress magnitude

Section		L125×8	L140×10	L160×10	L180×12	L200×14
β	Measured	0.09	0.13	0.08	0.10	0.12
	Ref. [23]	0.20	0.20	0.20	0.20	0.20
	Ref. [23]	0.25	0.25	0.25	0.25	0.25
	Ref. [23]	0.30	0.30	0.30	0.30	0.30

which is consistent with other test results (Rasmussen and Hancock 1995).

The average value of the residual stresses of every element is applied at its integration points as the initial stress for convenience and simplification in the FEA. Hence, the distribution and the magnitude of the residual stresses shown in Fig. 19 are adopted in the FEA.

The input of the residual stress in the FEA is accomplished in manner of the residual stress file, which is written by the external program such as FORTRAN. In this file, the residual stress of every element is stored in a two-dimensional array, whose rows and columns are equal to the integration points of the element and the components of the residual stress in number respectively. The residual stress file is read

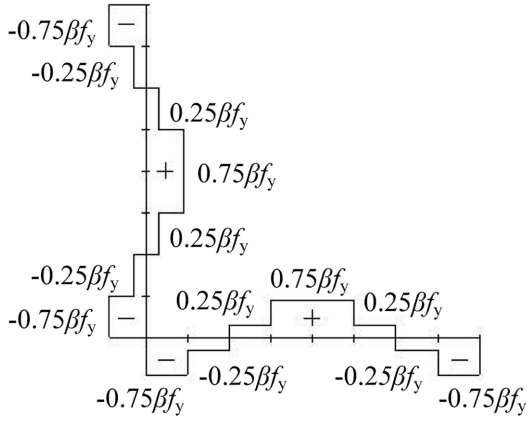

Fig. 19 Residual stress adopted in FEA

before the nonlinear buckling analysis and the input of the residual stress is done.

5.3. Verification of the finite element model

The FEA procedure includes 3 steps. Firstly, the finite element model without any geometric imperfection or residual stress is created, and both the displacement restraints and the axial compressive force are applied. Then a static solution is done to obtain the stiffness matrix of the model. Secondly, eigenvalue buckling analysis is conducted to obtain the buckling mode which is adopted as the initial geometric imperfection of the models in the subsequent nonlinear buckling analyses. Thirdly, after incorporating the geometric imperfections and the residual stresses, a nonlinear buckling analysis is carried out with the arc-length method to obtain the ultimate load carrying capacity of the model.

A comparison between the FEA results and the test results is shown in Table 8, where P_u denotes the test results and F_A denotes the FEA results. From Table 8 it is shown that the FEA results agree reasonably well with the test results and the difference is only 2% on average. Thus, the proposed finite element models are able to analyze the local buckling behavior of high strength steel equal angle columns under axial compression after incorporating the initial geometric imperfections and residual stresses, and they are readily applicable for further parametric studies.

6. Parametric study and design method

After the validation of the finite element model, a series of finite element parametric study is carried out to examine the effect of the geometric imperfections, the residual stresses and the width-to-thickness ratios of the angle section on the local buckling behavior of high strength steel equal angle columns under axial compression. The nominal values of all the dimensions of the specimens and the elastic-perfectly plastic material model are used in the parametric analyses. The nodes at the interface of the end plates and the angle column are coupled three translational degrees of freedom to relax the rotation of the angle end, which will make the ends of the angle legs pinned.

6.1. Geometric imperfection

Referred to the existing research data, corresponding literatures and codes, the range of the geometric imperfection is $w/250$, $w/100$ and $w/50$. 5 section sizes are selected, i.e., L125 × 8, L140 × 10,

Table 8 Comparison between FEA results and test results

Specimen	P_u (kN)			F_A (kN)			$\Delta = F_A/P_u$			
	x=1	x=2	x=3	x=1	x=2	x=3	x=1	x=2	x=3	Average
L125×8-x	854.9	817.1	851.5	815.1	815.7	822.6	0.953	0.998	0.966	0.973
L140×10-x	1181.3	1232.1	1224.1	1191.7	1188.6	1190.3	1.009	0.965	0.972	0.982
L160×10-x	1361.2	1415.3	1378.1	1378.9	1368.8	1375.1	1.013	0.967	0.998	0.993
L180×12-x	1904.4	1880.6	1829.4	1846.7	1857.4	1844.7	0.970	0.988	1.008	0.989
L200×14-x	2362.2	2348.8	2417.0	2288.0	2333.4	2286.5	0.969	0.993	0.946	0.969
Average							0.981			
Standard Deviation							0.021			

Table 9 FEA results with different geometric imperfections

Section	F_1 (kN)	F_2 (kN)	F_3 (kN)	F_1/F_2	F_3/F_2
L125×8	802.46	770.22	695.47	1.042	0.903
L140×10	1121.46	1105.40	1030.00	1.015	0.932
L160×10	1284.10	1221.00	1092.80	1.052	0.895
L180×12	1732.38	1681.50	1542.39	1.030	0.917
L200×14	2244.51	2203.20	2027.40	1.019	0.920
		Average		1.032	0.913

L160 × 10, L180 × 12 and L200 × 14. The distribution of the residual stress is shown in Fig. 19, and the peak value coefficient β is 0.3.

The FEA results are shown in Table 9, where F_1, F_2 and F_3 represent the ultimate loads of the angle columns with the geometric imperfections of w / 250, w / 100 and w / 50 respectively. From Table 9 it is shown that the ultimate loads decrease with an increase of the geometric imperfections, but the discrepancy, which increases with the increase of the width-to-thickness ratio, is not pronounced. Furthermore, base on the FEA results above and the recommendation in the Chinese code for acceptance of construction quality of steel structures (GB 50205-2001 2001), the geometric imperfection is w/100 in the following analyses.

6.2. Residual stresses

The distribution of the residual stresses is shown in Fig. 19, and three values of the peak value coefficient β are included in the study: 0.2, 0.25 and 0.3. 5 section sizes are selected, i.e., L125 × 8, L140 × 10, L160 × 10, L180 ×12 and L200 × 14. The FEA results are shown in Table 10, where F_1, F_2 and F_3 represent the ultimate loads with the peak value coefficient of 0.2, 0.25 and 0.3 respectively. From Table 10 it is shown that the influence of the residual stresses on the ultimate loads of the angle columns is fairly small, which is consistent with the existing research results. Besides, the peak value coefficient is 0.3 in the following analyses.

6.3. Width-to-thickness ratios

In general, the width-to-thickness ratios of the angle sections are the most important factor that influences the ultimate loads of the angle columns. The Chinese standard hot rolled section steel (GB/T 706-2008 208) includes 114 different angle sizes, of which the smallest width-to-thickness ratio w/t is 5.00 (L20 × 4) while the largest width-to-thickness ratio is 18.75 (L150×8). Hence, 14 different angle

Table 10 FEA results with different residual stresses

Section	F_1 (kN)	F_2 (kN)	F_3 (kN)	F_1/F_2	F_3/F_2
L125×8	773.91	772.19	770.22	1.002	0.997
L140×10	1107.96	1105.94	1105.40	1.002	1.000
L160×10	1226.42	1224.56	1221.00	1.002	0.997
L180×12	1687.29	1684.59	1681.50	1.002	0.998
L200×14	2207.43	2206.44	2203.20	1.000	0.999
		Average		1.002	0.998

Table 11 Sections and width-to-thickness ratios of steel angles

Section	L20×4	L100×16	L56×8	L40×5	L63×7	L200×20	L110×10
w/t	5.00	6.25	7.00	8.00	9.00	10.00	11.00
Section	L36×3	L160×12	L140×10	L180×12	L80×5	L70×4	L150×8
w/t	12.00	13.33	14.00	15.00	16.00	17.50	18.75

sizes with a full range of width-to-thickness ratios between 5.00 and 18.75 are selected for the parametric study, as presented in Table 11.

The representative failure mode of the angle column from the FEA is shown in Fig. 20. The nondimensional FEA results are plotted as the FEA curve in Fig. 21, from which it is shown that the ultimate stresses decrease with an increase of the width-to-thickness ratio. When the width-to-thickness ratio is less than 10 (6 section sizes), the ultimate stresses are rather constant. However, once the width-

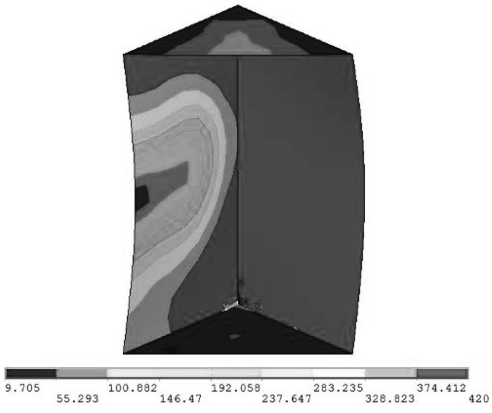

Fig. 20 Steel angle failure mode

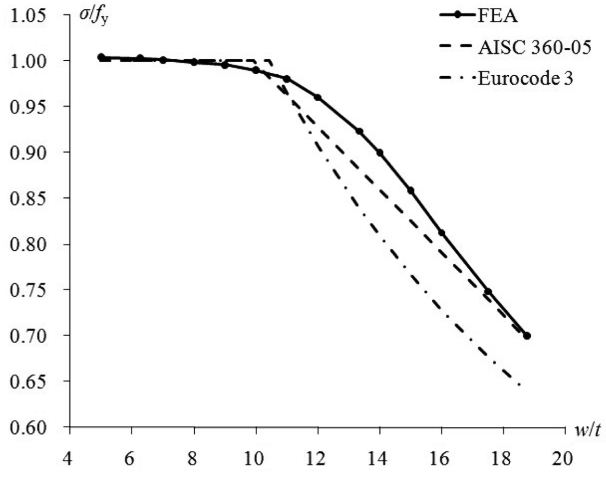

Fig. 21 Comparison between nondimensional FEA and design strengths

to-thickness ratio exceeds 10 (8 section sizes), the ultimate stresses decrease rapidly. Thus, the influence of the width-to-thickness ratio on the ultimate load of 420 MPa high strength steel equal angle columns under axial compression is significant at the range of large width-to-thickness ratios.

The comparison between nondimensional FEA and design strengths by ANSI/AISC 360-05 (2005) and Eurocode 3 (EN 1993-1-5 2006, EN 1993-1-1 2005) is shown in Fig. 21, from which it can be seen that the ANSI/AISC 360-05 and Eurocode 3 curves both consist of two parts: the horizontal segment and the decreasing segment. For the horizontal segment, the difference between FEA results and the design strengths by ANSI/AISC 360-05 and Eurocode 3 is reasonably small, and the three curves almost coincide completely. For the decreasing segment, ANSI/AISC 360-05 and Eurocode 3 both conservatively predict the strength, but the discrepancy is smaller for ANSI/AISC 360-05.

Base on the analysis above, it is concluded that ANSI/AISC 360-05 can more accurately predict the local buckling strength of 420 MPa high strength steel equal angle columns under axial compression than Eurocode 3, and for the design method by Eurocode 3, the local buckling design strength of 420 MPa high strength steel equal angle columns under axial compression can be enhanced appropriately at large width-to-thickness ratio values. Thus the design method by ANSI/AISC 360-05 is recommended in this paper to predict the local buckling strength of 420MPa high strength steel equal angle columns under axial compression.

7. Conclusions

An experiment on the local buckling of 420 MPa high strength steel equal angle columns under axial compression has been conducted. The test results are compared with the corresponding design strengths in ANSI/AISC 360-05 and Eurocode 3. Then the finite element model is developed and validated by the test results. After that, the finite element parametric analysis is conducted and the results are compared with the design strengths by ANSI/AISC 360-05 and Eurocode 3. Based on the research work above, the following conclusions have been drawn:

(1) The local buckling is significant and must be considered for the 420 MPa high strength steel equal angle columns under axial compression with small slenderness, whose width-to-thickness ratio values exceed the limit value.

(2) The test results are higher than the design strengths of ANSI/AISC 360-05 and Eurocode 3, and with the increase of the width-to-thickness ratio, the excess range becomes larger. The design methods of ANSI/AISC 360-05 and Eurocode 3 can predict sufficiently safe results for the local buckling of 420MPa high strength steel equal angle columns under axial compression, whose width-to-thickness ratio values exceed the limit value.

(3) The finite element model created in this paper can accurately simulate the initial geometric imperfection and residual stress of the specimens, analyze the local buckling behavior of the 420 MPa high strength steel equal angle columns under axial compression, and be used for the further parametric study.

(4) The influence of geometric imperfection and residual stress on the local buckling strength of 420 MPa high strength steel equal angle columns under axial compression is smaller than it is for ordinary strength steel, which is consistent with the existing research results. The influence of the width-to-thickness ratio on the local buckling strength of 420 MPa high strength steel equal angle columns under axial compression is significant at the range of large width-to-thickness ratios.

(5) By comparing the FEA results with the design strengths of ANSI/AISC 360-05 and Eurocode 3, it is concluded that ANSI/AISC 360-05 can more accurately predict the local buckling strength of

420MPa high strength steel equal angle columns under axial compression than Eurocode 3, and the design method by ANSI/AISC 360-05 is recommended.

Acknowledgements

This work was jointly supported by the National Natural Science Foundation of China (No. 50708051) and Program for Changjiang Scholars and Innovative Research Team in University (IRT0736).

References

ABAQUS Theory Manual (2003), Version 6.4. Pawtucket, Hibbit, Rhode Island, Karlsson and Sorensen Inc.

ANSI/AISC 360-05 (2005), *Specification for Structural Steel Buildings*, American Institute of Steel Construction, Chicago.

ANSYS Multiphysics 10.0 (2003), Ansys Inc., Canonsburg, Pennsylvania.

AS 4100 (1998), *Steel Structures*, Standards Association of Australia, NSW.

Ban, H.Y., Shi, G., Shi, Y.J. and Wang, Y.Q. (2009), "Experiments on the residual stress of 420MPa steel equal angles", *Proceedings of the Sixth International Conference on Advances in Steel Structures*, Hong Kong, China, December.

Clarin, M. and Lagerqvist, O. (2005), "Plate buckling of high strength steel - Experimental investigation of welded box section under compression", *Steel Members and Structural Systems*, Eurosteel Maastricht, Volume A, 1.4, 207-214.

Code for design of steel structures committee (2003), *Application Construal of Code for Design of Steel Structures in China*. China Planning Press, Beijing. (in Chinese)

Dwight, J.B. and Moxham, K.E. (1969), "Welded steel plates in compression", *Struct. Eng.*, **47**(2), 49-66.

EN 1993-1-1 (2005), *Eurocode 3: Design of steel structures - Part 1-1: General rules and rules for buildings*, European Committee for Standardization, Brussels.

EN 1993-1-5 (2006), *Eurocode 3: Design of steel structures - Part 1-5: Plated structural elements*, European Committee for Standardization, Brussels.

GB 50017-2003 (2006), *Code for Design of Steel Structures*, China Architecture and Building Press, Beijing.

GB 50205-2001 (2001), *Code for Acceptance of Construction Quality of Steel Structures*, China Planning Press, Beijing. (in Chinese)

GB/T 228-2002 (2002), *Metallic Materials-Tensile Testing at Ambient Temperature*, Standards Press of China, Beijing. (in Chinese)

GB/T 2975-1998 (1998), *Steel and Steel Products-Location and Preparation of Test Pieces for Mechanical Testing*, Standards Press of China, Beijing. (in Chinese)

GB/T 706-2008 (2008), *Hot Rolled Section Steel*. China Planning Press, Beijing. (in Chinese)

Hermann, S.D. (2002), "On the local stability interaction effect of high strength steel columns", *Steel Members and Structural Systems*, Eurosteel Coimbra, 353-360.

IABSE (2005), *Use and Application of High-performance Steels for Steel Structures*, IABSE, Zurich,

Switzerland.

Nishino, F., Ueda, Y. and Tall, L. (1967), "Experimental investigation of the buckling of plates with residual stresses, tests methods for compression members", *ASTM Special Technical Publication No. 419*, ASTM, Philadelphia, PA, 12-30.

Pocock, G. (2006), "High strength steel use in Australia, Japan and the US", *Struct. Eng.*, **84**(21), 27-30.

Rasmussen, K.J.R. and Hancock, G.J. (1992), "Plate slenderness limits for high strength steel sections". *J. CONSTR. STEEL. RES.*, **23**(1-3), 73-96.

Rasmussen, K.J.R. and Hancock, G.J. (1995), "Tests of high strength steel columns", *J. CONSTR. STEEL. RES.*, **34**(1), 27-52.

Shi, G. and Bijlaard, F.S.K. (2007), "Finite element analysis on the buckling behavior of high strength steel columns", *Proceedings of the Fifth International Conference on Advances in Steel Structures*, Singapore, December.

Tang, L.R.B. and Mahendran, M. (2004), "Behavior of high strength steel compression members", *Proceedings of 10th Nordic Steel Construction Conference*, Copenhagen, Denmark.

Usami, T. and Fukumoto, Y. (1982), "Local and overall buckling of welded box columns", *J. Struct. Div.*, **108**(3), 525-542.

CC